AE8144 Computational Methods in Aerodynamic Analysis

Term Project Report

Fall 2024

Free Convection Flow and Heat Transfer in a vertical Cylinder with Circular Fins of Triangular Cross-Section

Instructor: Dr. Paul Walsh

Student Name: Aman Gilani

Student ID: 500879895

Abstract

This study focuses on the numerical analysis of natural convection heat transfer in a vertical hollow cylinder with circular fins of triangular cross-section using Computational Fluid Dynamics (CFD). The investigation explores multiple grid types—linear, non-linear, and multi-block grids—to assess their impact on heat transfer rates, represented by the Nusselt number and heat flux. Simulations were conducted using structured, semi-structured, and multi-block meshes, with the grid resolutions varying between 19,918 (coarse) and 315,720 (fine) cells. The study also includes transient unsteady calculations over 2,000-time steps of 1 second each. Results demonstrate that a finer structured grid (element size = 0.05 m) yields a lower Nusselt number of 60.75, compared to 70 for a coarse structured grid (element size = 0.2 m). The finer mesh showed an average fluid temperature of 343.6 K and a heat flux of -322.8 W/m².

Semi-structured grids, particularly with a non-linear mesh aligned with the heated cylinder boundary, improved solution accuracy near the cylinder walls, yielding a Nusselt number of 68.1. The implementation of multi-block grids further optimized computational efficiency, with semi-circular and rectangular meshes producing comparable Nusselt numbers of 68.7 and 68.8, respectively. A grid convergence index (GCI) for the finest grid was computed as 0.175 for the Nusselt number and 0.112 for heat flux, validating the grid-independent solution. A grid-independent heat flux was calculated to be -293.3 W/m^2, and a grid-independent Nusselt number was calculated to be 52.2.

This research studies the trade-offs between computational cost and numerical accuracy in various grid generation techniques and lays the groundwork for incorporating adaptive meshing and multi-time-stepping techniques in future analyses.

Table of Contents

List of Figures

List of Tables

Introduction

Heat sinks are passive heat exchangers that play a fundamental role in the thermal energy management of an electronic, thermal, or mechanical device. Heat sinks are designed to dissipate excess heat generated by these devices into a fluid medium, often air or a liquid coolant, to allow safe operation, reliability, and temperature regulation of the device. Heat sinks are extensively used in a wide range of applications where consistent and reliable dissipation of heat is crucial for the device's operation. For instance, from power systems and electronics of an aircraft system to industrial machinery, nuclear reactors, and air coolers, heat sinks are designed and optimized to maximize heat dissipation and temperature regulation of the device or system. Amongst a diverse assortment of heat sinks for various purposes, this paper aims to analyze the natural convection heat transfer features of a vertical, hollow, cylindrical heat sink with triangular fins.

Throughout the development of cylindrical heat sinks, several numerical and experimental investigations have been performed to study their natural and forced convection properties. A forced convection analysis of a vertical heat sink demonstrates a faster heat transfer rate due to the non-zero velocity of the fluid medium. On the other hand, the study of natural convection in a heat sink streamlines several assumptions since there are no moving walls in the computational model. Thus, studying natural convection heat transfer processes becomes computationally more reliable, cost-efficient, and consumes less time and energy. To increase the heat transfer rate of a cylindrical heat sink, different shapes of fins can be studied by placing them on the outer surface of the heat sink wall. This leads to an increased surface area to volume ratio of the heat sink, which leads to a higher heat transfer process. A vertical, hollow, cylindrical heat sink designed for this study features a central core that is maintained at a constant temperature of 400 K. The fins extend outward radially, featuring a triangular cross-section. The vertical orientation of the heat sink enhances the natural convection heat transfer process by influencing the airflow due to the buoyance-driven effects of the fluid medium.

There has been an extensive amount of research conducted on such heat sink designs, studying multiple fin shapes and optimal fin radial length to improve the overall heat transfer rate of the system. Such studies include J.R. Senapati et al. [1], where the authors study the natural convection heat transfer of a vertical cylinder with annular fins numerically. The authors have done this by varying Rayleigh numbers in laminar and turbulent regimes. Furthermore, the study

optimizes the fin spacing for maximum heat transfer in a fully turbulent flow. An et al. [2] experimentally studies the natural convection over a vertical cylinder with plate fins. This study also draws motivation from Kimura et al. [3], where the authors experimentally investigate the natural convection through water induced around a heated vertical cylinder. Acharya et al. [4] also revisited the natural convection heat transfer from a vertical hollow cylinder suspended in air through a numerical analysis.

The objective of this numerical study is to investigate the unsteady, transient state, free (natural) convection heat transfer process, and the flow structure over a vertical, hollow cylinder with circular fins of the triangular cross-section. Moreover, the numerical analysis will focus on exploring the effects of linear, nonlinear, and multi-block grids for turbulent flows. The results of this study will be validated using a grid convergence study that compares the Nusselt number and heat flux for different computational grids. Additionally, the results are also compared to the above-mentioned investigations to gain validity for the designed numerical investigation. The following section of this paper details the assumptions, boundary conditions, initial conditions, and the model setup for the transient state analysis of the heat sink model on ANSYS Fluent.

Model Construction

The problem description for this study includes a heated vertical cylinder with circular fins of a triangular cross-section that undergoes a natural convection heat transfer. **Figure 1** below illustrates an isometric view and a front view of the hollow cylinder with five fins placed equidistant from each other. The flow around the heat sink is modeled as unsteady, transient, turbulent, and two-dimensional (2D) axisymmetric. The material for the heated surface of the heat sink is designed with aluminum due to its high conductivity, as seen in **Table 1**. For this study, the fluid medium was chosen to be air with zero velocity. Moreover, the temperature changes throughout the transient analysis are expected to occur in small increments. Therefore, the density of the fluid medium is modeled as an incompressible ideal gas. This then leads to the mass conservation equation being solved pressure-based since there is no fluid phase change or density changes during the natural convection heat transfer through the fluid medium.

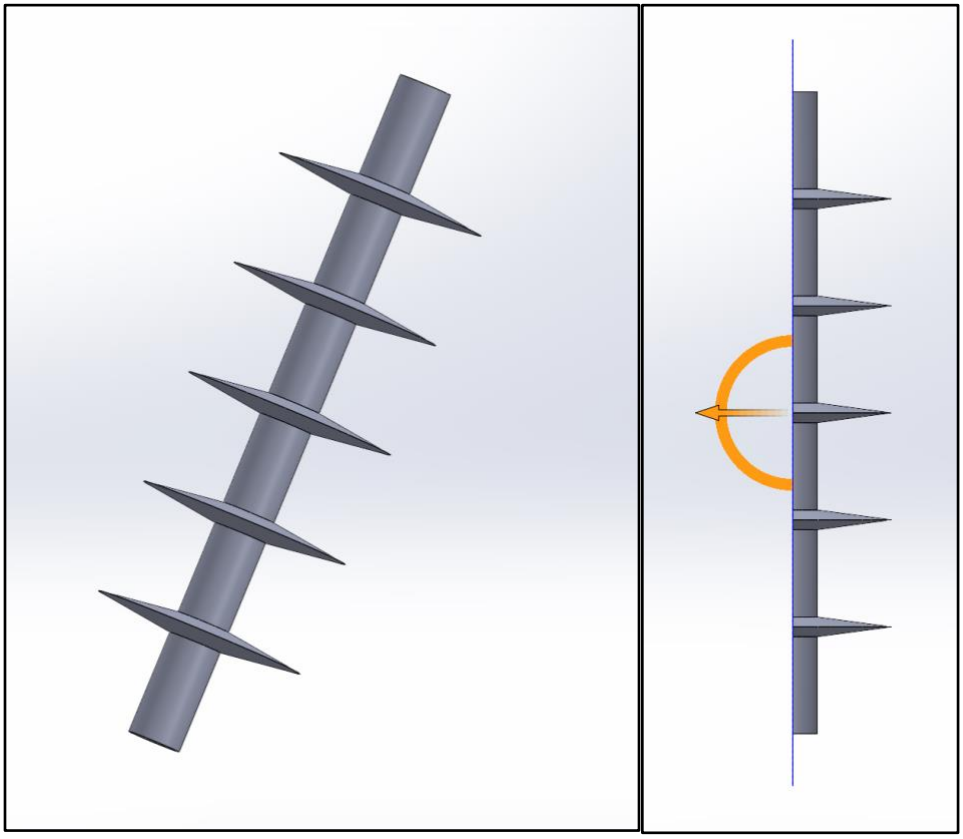

Figure 1: *Heat Sink with Circular Fins of Triangular Cross-section. (Left: Isometric View, Right: Front View.)*

The following table tabulates the material properties of aluminum (used for the heated walls) and air (used as the fluid medium) for this analysis.

Table 1: *Material Properties.*

	Aluminium (Heated Wall)	Air (Fluid Medium)
Density	2719 kg/m^3	1.225 kg/m^3 Incompressible Ideal Gas
Specific Heat (Cp)	871 J/(kg K)	1006.43 J/(kg K)
Thermal Conductivity	202.4 W/(m K)	0.0242 W/(m K)
Viscosity	-	1.7894e-05 kg/(m s)

Boundary Conditions and Initial Conditions.

The numerical simulation of natural convection heat transfer on a vertical cylinder with circular fins is implemented using a two-dimensional axisymmetric geometry, as evident from **Figure 2**. As seen, the surface of the heated cylinder and the fins are modeled as isothermal walls at a constant temperature of 400 K. The surrounding walls of the computational domain are also modeled as isothermal walls maintained at 293 K, and the fluid medium (Air) is maintained initially at a room temperature of 293 K, which is the standard practice in the industry. The Prandtl number (Pr) for air is calculated to be 0.744 using the equation below.

$$Pr = \frac{\mu C_p}{k}$$

To add another dimension to the project, the walls could also be modeled with varying surface temperatures using a linear or non-linear temperature equation during the model setup. However, this was not considered for the course of the study to simplify and streamline the simulations. In addition, the value for gravity is set to be ten m/s^2 in the negative x-axis, as seen in the diagram below, mainly for computational ease.

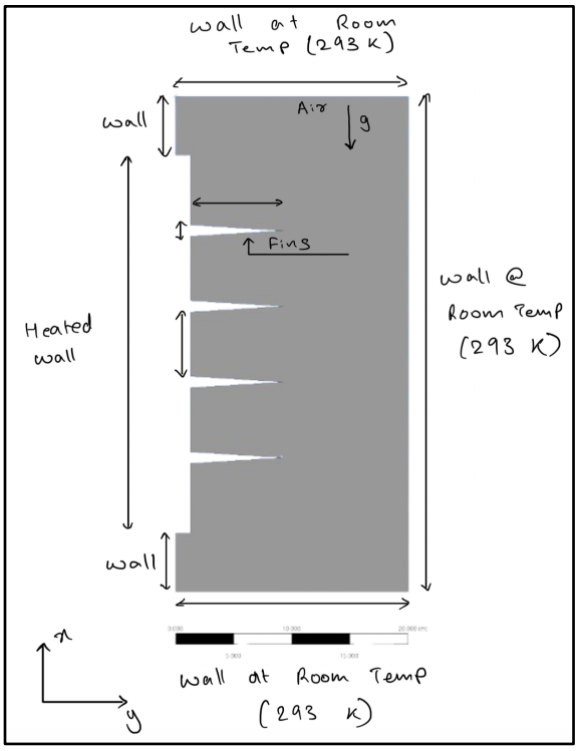

***Figure 2**: Schematic Diagram of the Computational Domain with Boundary Conditions.*

The following table tabulates the boundary conditions of the heatsink wall (cylinder and fins) and the surrounding walls, as seen in **Figure 2**.

***Table 2**: Boundary Conditions and Initial Conditions.*

	Heat Sink Wall	Surrounding Wall	Fluid Medium
Material	Aluminium	Aluminum	Air
Thermal Boundary Condition	Isothermal wall at 400 K	Isothermal wall at 293 K	Initially at 293 K.
Shear Boundary Condition	No-slip	No-slip	-
Wall Motion	Stationary wall	Stationary wall	Zero fluid velocity initially
Heat Generation Rate [W/m^3]	0	0	0

The wall motion for the heat sink wall and the surrounding walls in the computational domain are modeled as stationary walls because this paper aims to study the natural convection heat transfer. No heat generation sources or sinks have been considered for the course of this project. Thus, the cylinder wall temperature is assumed to be at 400 K at time = 0. Additionally, the walls are modeled with no-slip shear boundary conditions. The pressure outside the computational domain is set as a standard atmospheric pressure of 1 atm.

Mesh Development

The computational domain illustrated in **Figure 2** highlights the geometry used for the course of this analysis. The geometric model is then used to develop different types of meshes. The objective of this study is to explore three sizes of linear mesh, a non-linear mesh, and two types of multiblock grids. Using the above-mentioned grid types is an opportunity to study and compare the natural convection heat transfer along with the computational feasibility and effort required to implement them. It is expected that a non-structured grid should be able to yield a more accurate solution, however, at a higher cost in terms of computational time and energy. The implementation of multiblock grids is expected to reduce errors prone to element sizing by creating a super-fine mesh in this region and a restively coarse mesh in other areas.

Linear Mesh

A linear mesh, also known as structured mesh, is created using a mix of 2D quadrilateral and triangular shape elements with varying sizing. The element size ‘h’ is reduced by a factor of 2 to obtain each new mesh. As the mesh size decreased, the computational time to generate the mesh increased. For this analysis, three linear grids are created with sizes 0.2, 0.1, and 0.05 m, highlighted in **Figure 3**.

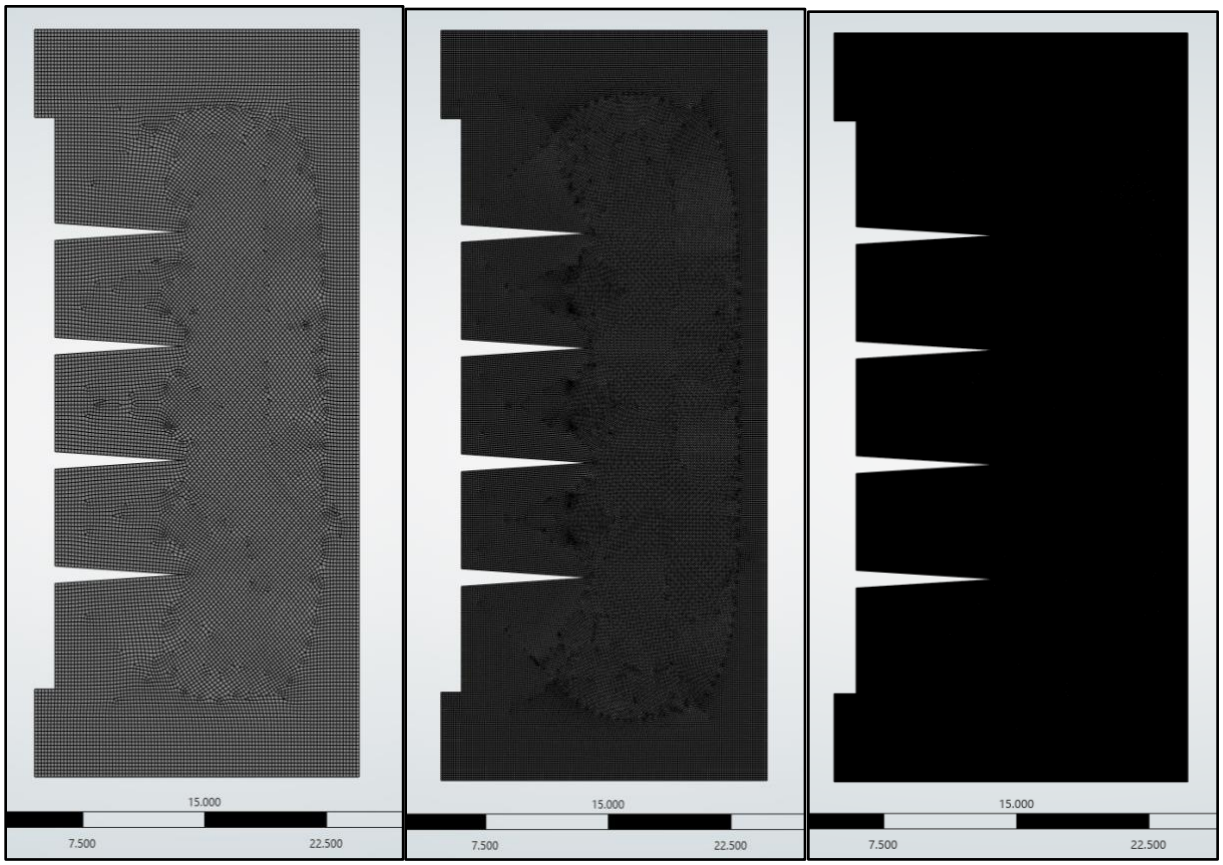

***Figure 3**: Linear Structured Mesh. (Left: h = 0.2, Center: h = 0.1, Right: h = 0.05.)*

As seen in the above figure, as the element size decreases, the mesh becomes more populated with an increasing number of cells. Increasing the number of cells provides a more accurate result and is better at resolving flow features. **Table 3** below tabulates the element sizes for coarse, medium, and fine meshes and their respective number of cells and nodes.

***Table 3:** Linear Structured Mesh Sizes.*

	Element Size	No. of Cells	No. of Nodes
Coarse Mesh	0.2 m	19918	20363
Medium Mesh	0.1 m	79289	80158
Fine Mesh	0.05 m	315720	317446

Non-Linear Mesh

The second type of mesh generated for this analysis is a non-linear grid. This type of mesh is also known as a semi-structured grid. The non-linearity of the grid is evident along the boundary of the hot cylinder wall, as seen in **Figure 4.** An element size of 0.2 m is used for the structured grid inside the fluid medium domain, and a very fine mesh is used along the cylinder wall and fin edge with 250 divisions. The non-linear grid consists of 45704 no. of cells and 46433 no. of nodes.

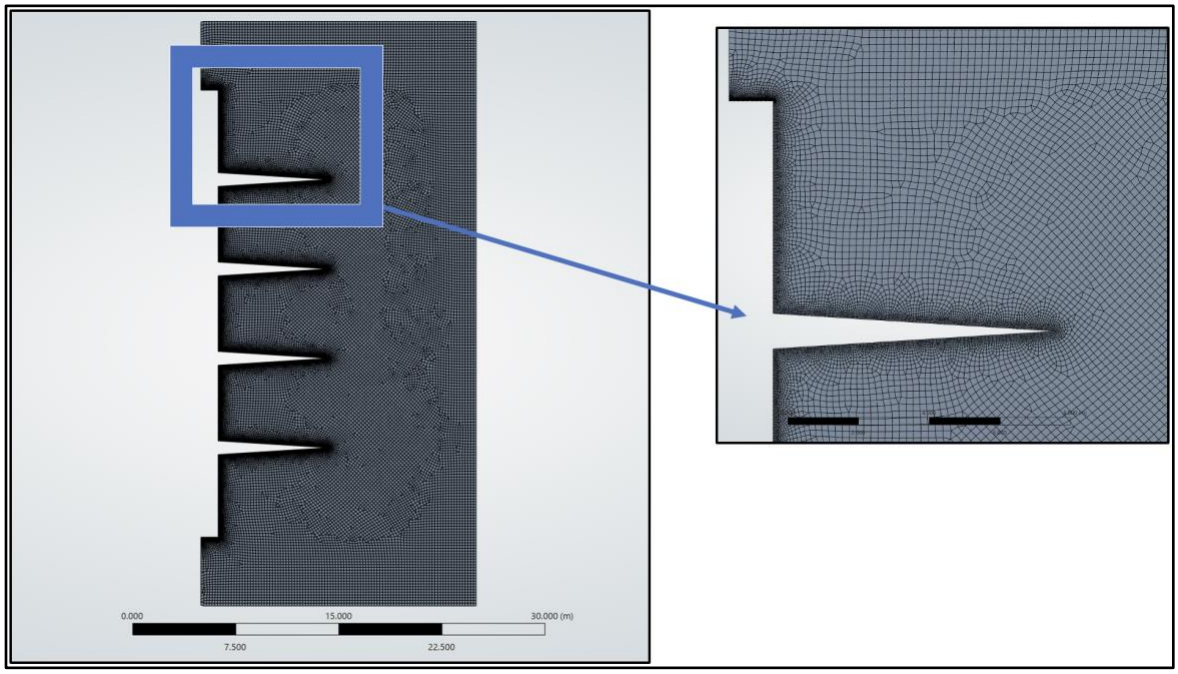

Figure 4: *Semi-Structured Mesh, Non-Linear Boundary Mesh.*

Multi-Block Grids

Lastly, two multiblock grids are created with two different shapes of fine meshes concentrated in the center of the computational domain. For this study, rectangular and semi-circular fine meshes are created as evident in **Figure 5** below. In the structured region an element size of 0.2 is again utilized to maintain consistency for both multiblock grids and a refinement factor of 2 is used for the fine meshes in the respective shapes.

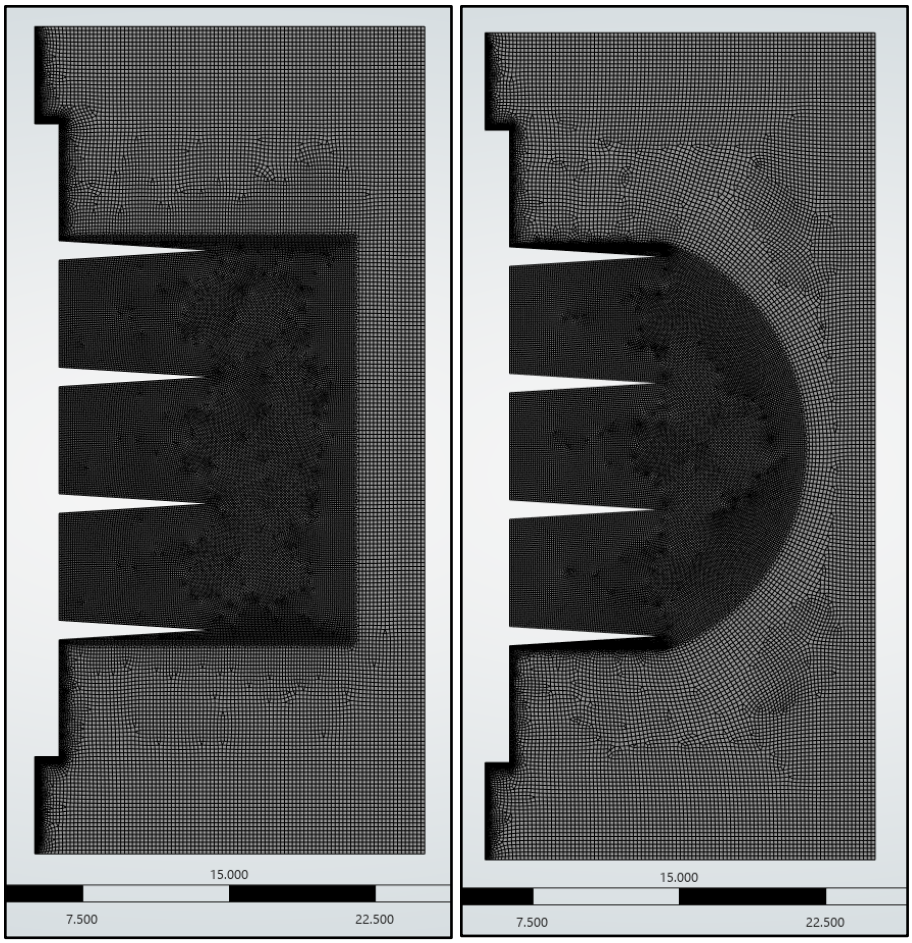

Figure 5: *Multi Block Grids, (Left: Rectangular, Right Semi-Circular).*

The development of the multiblock grids required a slight update to the original geometry. The grids were created by first creating a face respective to a rectangular block and a semi-circular block in the design modeler. These faces were then used to create the fine meshes using the above-mentioned refinement factor.

Additionally, it is recorded that by changing, changing the shape from a rectangular fine mesh to a semi-circular fine mesh, the number of cells and nodes decreased substantially. The above grids are computed using a mix of 2D quadrilateral and triangular-shaped elements. The decision to create the above-illustrated grids was made after viewing the solutions for temperature distribution for a structured grid. It was recorded that, the static temperature had large fluctuations near the boundary of the hot cylinder wall and toward the center of the computational domain.

Table 4: *No. of Cells & No. of Nodes for Different Types of Mesh in Increasing Cell Number.*

	No. of Cells	No. of Nodes
Linear Mesh – Coarse	19,918	20,363
Non – Linear Mesh	45,704	46,433
Multi Block Grid - Semi circular	47,277	48,150
Multi Block Grid – Rectangular	51,153	51,650
Linear Mesh – Medium	79,289	80,158
Linear Mesh – Fine	315,720	317,446

Table 4 above tabulates the number of cells and number of nodes for each grid type in an increasing cell number. It was recorded that a coarse linear mesh has the least number of cells. For the same element size, introducing a source of non-linearity at the boundary or in the form of a fine mesh block, the number of cells increases. The effect of this is compared in later sections wherein the average Nusselt number is compared for different computational grids. It is expected that creating a fine mesh block in a concentrated region increases the solution accuracy.

Ansys Model Setup

The flow around the vertical cylinder with circular fins of a triangular cross-section is modeled as 2nd order implicit unsteady in time to maintain system stability. The flow is determined to be laminar or turbulent depending on the Rayleigh number and the fluid medium is assumed to be incompressible ideal gas. In general, flow with a Rayleigh number greater than 10^9 is considered turbulent. The modeling of turbulence in the computational domain is implemented using Reynolds Averaged Navier-Stokes (RANS) equations coupled with a two-equation eddy viscosity-based standard K – ϵ turbulence model. The enhanced wall treatment is enabled for this study to enable near-wall modeling of the viscous sublayers forming in the computational domain.

However, this is not necessary in a model where the mesh is sufficiently fine everywhere. The enhanced wall treatment model is used to ensure that the first near-wall node is placed completely either in a laminar or turbulent regime. Since the velocity of the fluid medium is set as zero initially, the computational domain has a non-rotating flow and thus the absolute velocity formulation is used to calculate the flow speed.

The fundamental mass and momentum conservation equations and the energy equations dictating the fluid flow and heat transfer for this investigation are calculated using their cartesian form. Since the natural convection process occurs inside a closed domain, such as one designed for this study, buoyancy is induced due to the force of gravity acting within the computational domain, this creates small variations of density and temperatures in the fluid medium. The Boussinesq model is used to achieve faster convergence rates. This is reflected in the maximum number of iterations set per time step in **Table 5**. This model sets the density as a constant parameter and introduces a buoyancy parameter in the momentum equation. The density is computed at time = 0, at a reference average temperature between the hot cylinder wall and the surrounding atmospheric room temperature. This value is set as a constant and any density variations due to the temperature changes are modeled using the Boussinesq parameter. This is a reasonable assumption for this investigation since the temperature fluctuations are not very large in the computational domain.

The transient flow calculation parameters for the model are tabulated in **Table 5**. The unsteady solutions for this problem are computed across 33 minutes with an interval of 1 sec. Even though the temperature fluctuations are expected to be small for this simulation, a transient calculation is performed to ensure the total mass is conserved and also to understand and experience multiple time-stepping functions in the ANSYS fluent software.

Table 5: *Unsteady Calculation Parameters.*

Unsteady Calculation Parameters	
Number of time steps	2000
Time step size	1 sec
Max iteration per time step	40

For the course of this project, as established earlier, a pressure-based type solver is utilized along with successive under-relaxation factors for equations to control the computation of each variable throughout the multiple iterations in a time step. In general, under relaxation factors are used to maintain systemic stability. The under-relaxation parameters for various equations are tabulated in **Table 6**. For this study, it was seen that if the under-relaxation parameters are decreased the momentum residuals grow and the system doesn't converge within the specified maximum number of iterations. For this study, the under-relaxation factors are enabled only for pressure, momentum, turbulent kinetic energy, and turbulent dissipation rate equation formulations. The energy and turbulent viscosity equation formulations do not have an under-relaxation term.

Table 6: *Under Relaxation Parameters.*

Under Relaxation Parameters	
Pressure	0.3
Momentum	0.7
Turbulent kinetic energy	0.8
Turbulent dissipation rate	0.8

A SIMPLE algorithm is used for velocity-pressure coupling which uses velocity and pressure correction factors to ensure conservation of mass. The discretization schemes for the study are tabulated in **Table 7** below. The majority of equation formulations use a second-order Upwinding scheme except when formulating pressure equations. A second-order scheme is preferred to increase the solution accuracy and reduce any error caused by the grid sizing. To analyze the turbulent flow, using the RANS solver, a second-order Upwinding scheme is also preferred to avoid false diffusion errors if the mesh is not sufficiently refined with the direction of flow or temperature changes.

***Table** 7: Discretization Scheme.*

Discretization Scheme	
Pressure	Second Order
Momentum	Second Order Upwinding
Turbulent Kinetic Energy	Second Order Upwinding
Turbulent Dissipation Rate	Second Order Upwinding
Energy	Second Order Upwinding

For the course of this study, the objective is to compare the natural convection heat transfer in the designed computation domain of a heated cylinder with fins while exploring the use of multiple types of grids – linear, non-linear, and multiblock grids. The natural convection heat transfer solutions for multiple grids showcased in the above section are compared using the average Nusselt number, which is a dimensionless number defined as the ratio of the convective heat transfer rate to the conductive heat transfer rate of a system. For this project, the Nusselt number is calculated at each time step using the following equation at x = 0.4 m calculated from the cylinder wall. The average Nusselt number is then calculated using an area-weighted average over the computational domain. The total heat transfer rate and the average temperature are computationally commuted over the fluid domain.

$$Nu = \frac{Qx}{k(T_{avg} - T_{\infty})}$$

Where,

- **x** is the location measured from the cylinder wall in the positive y direction.
- **Q** is the total surface heat flux measured as an area weighed average over the domain.
- $\mathbf{T_{avg}}$ is the average temperature measured as a volume-weighted average over the domain.
- **k** is the conductivity of air as given in **Table 1**.
- $\mathbf{T_{inf}}$ is the surrounding temperature of the cold wall as given in **Table 2**.

The Rayleigh number is another dimensionless number of importance that characterizes the effects of buoyancy and viscosity within a given fluid medium. For buoyancy-driven flows such as the one designed for this study, the Rayleigh number is an important parameter along with Nusselt number to define the natural convection heat transfer process. The Rayleigh number is calculated at x = 0.4 m.

$$Ra = \frac{g * \beta * x^3 (T_{avg} - T_\infty)}{\nu * \alpha}$$

Where,

- **x** is the location measured from the cylinder wall in the positive y direction.
- **g** is the constant of gravity as defined as 10 m/s^2.
- $\boldsymbol{\beta}$ is the thermal expansion coefficient which can be approximated by 1/T at the location x.
- $\boldsymbol{\nu}$ is the kinematic viscosity coefficient of the fluid medium air as defined in **Table 1**.
- $\boldsymbol{\alpha}$ is the thermal diffusivity of the fluid medium described as:

$$\alpha = \frac{k}{\rho * C_p}$$

Results

In this investigation, a numerical simulation of the Reynolds Averaged Navier Stokes equation coupled with the energy equation has been solved for a heated vertical cylinder with circular fins of triangular cross-section in a fluid medium. The simulation is conducted for five different grids as discussed earlier and the variation in the fluid Nusselt number is compared across different grids. The visualization of the temperature plume and the fluid flow over the vertical heat sink are also computed for each grid and presented in this section. Through this, the results will help understand the effect of different grid generation techniques on the natural convection heat transfer process and the fluid Nusselt number.

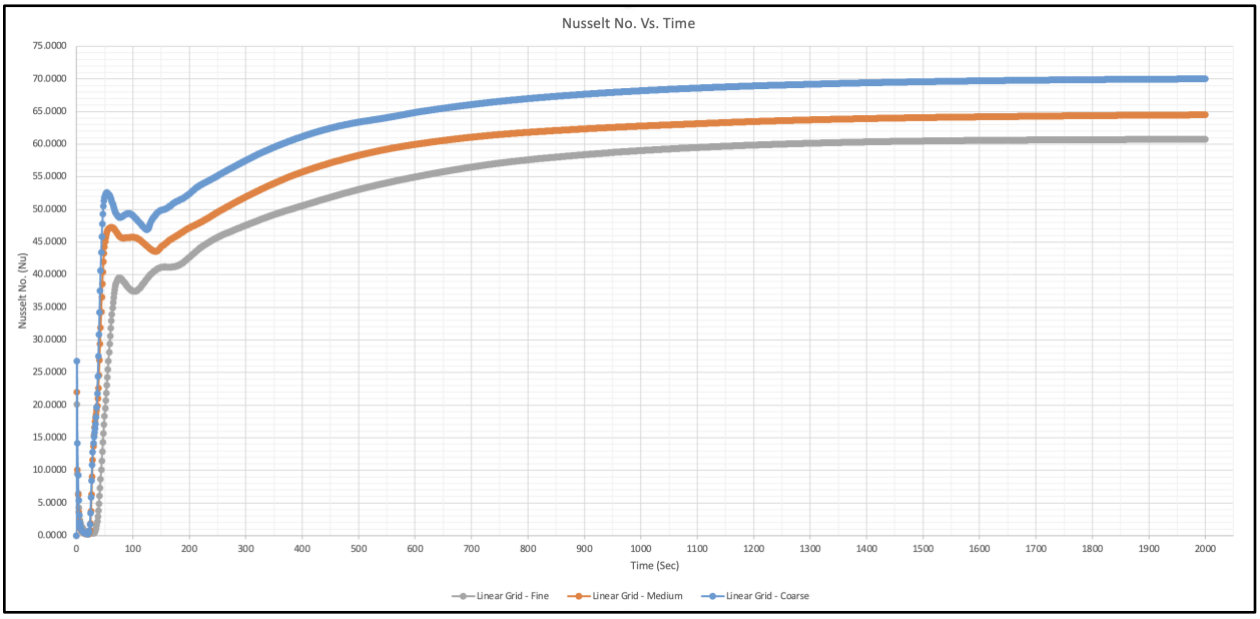

Figure 6: *Nusselt Number vs. Time-Transient Solution for Linear Grids.*

Figure 6 above plots the Nusselt number as a function of time as a result of the transient problem. The plot compares the transient solution for three linear grids. As evident on the plot, the finest grid produces a Nusselt number lower than that computed from a coarse and medium grid. As the element size decreases, the computational cells increase, and the Nusselt number is decreased. At time = 2000 s, the finest grid (h = 0.05) produces a Nusselt number of 60.75 with an average temperature of 343.6 K and a heat flux of -322.8 W/m^2. This trend is expected because, a finer mesh, can capture the temperature and heat transfer gradients more accurately.

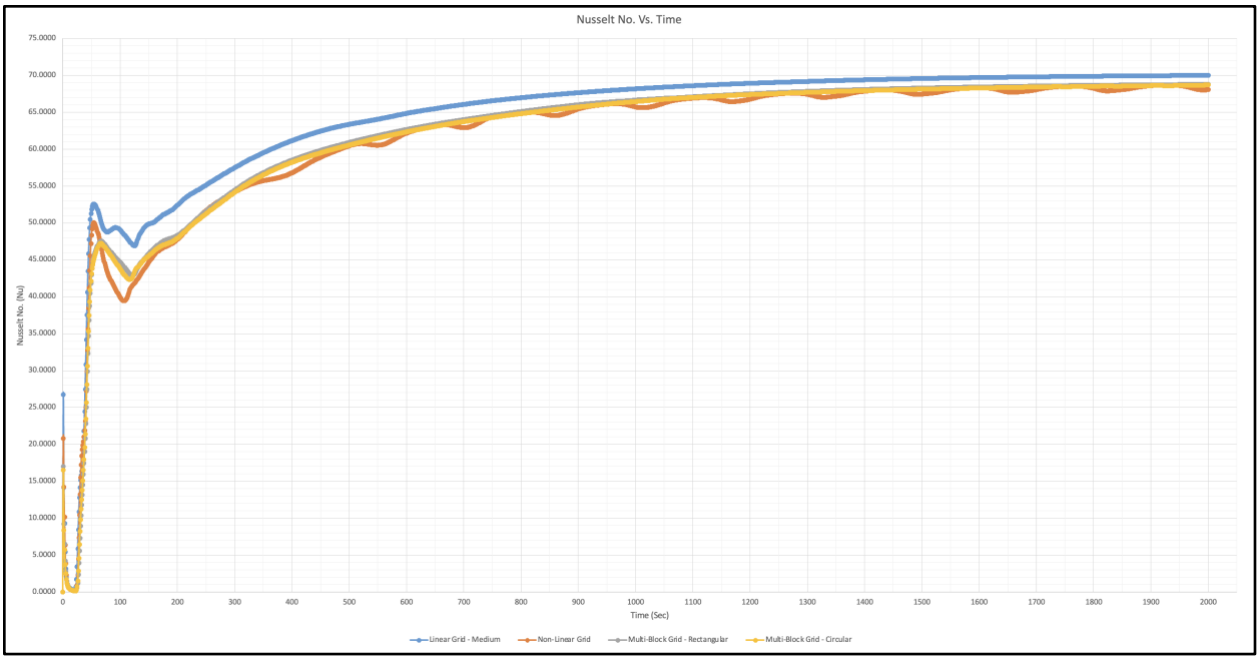

***Figure** 7: Nusselt Number vs. Time-Transient Solution for Non-Linear Grids.*

Figure 7 above plots the Nusselt number as a function of time as a result of the transient problem. The figure compares the Nusselt number computed using a coarse linear grid (h = 0.2) to the Nusselt number calculated using the non-linear, and the rectangular and circular multi block grids. The Nusselt number calculated using the coarse grid is 70. It is seen that the Nusselt number decreases when the mesh formulation shifts from structured to non-structured grids.

For the non-linear grid, the cells are closely packed along the boundary of the heated cylinder wall. This increases the solution accuracy as learnt from previous analysis. However, we can see some oscillations in the solution. Since the computational cells are closely packed along the hot cylinder wall, the boundary layer is captured with more accuracy. The resulting oscillations could be occurring because of laminar and turbulent regions forming inside the hot wall boundary layer with increasing time. The Nusselt number calculated using a non-linear edge grid is 68.1.

Comparing the coarse grid solution with an element size of 0.2 to a non-linear mesh the temperature, heat flux, and Nusselt number values decrease significantly. This is expected because relatively a greater number of computational cells are present along the heated cylinder wall.

However, when evaluating the multiblock grids the oscillations disappear because the fine mesh is extended well above the boundary layer. The Nusselt number calculated using a semi-circular multi-block grid is 68.7 and the Nusselt number calculated using a rectangular multi-block grid is 68.8. As recorded in **Table 8**, for the multi-block grid analysis, the variation in average temperature, Nusselt number, and heat flux are fairly consistent. Therefore, studying either of the two multiblock grids does not benefit any understanding of the heat transfer process as compared to the linear and non-linear grids seen above.

Table 8: *Average Temperature, Heat Flux, and Nusselt Number for Various Grids.*

Mesh Type		No. of Cells	Temperature	Heat Flux	Nusselt No.
Structured Mesh					
Linear Mesh	Coarse	19918	343.8	-373.3	70
	Medium	79289	343.5	-341.8	64.5
	Fine	315720	343.6	-322.8	60.7
Unstructured Mesh					
Unstructured Mesh	Non-linear	45704	340.6	-340.5	68.1
	Multiblock - Rectangular	51153	342	-353.6	68.8
	Multiblock - Semicircular	47277	341.9	-353	68.7

Figure 8 and **Figure 9** illustrate the temperature contour plots for structured and unstructured grids respectively. As seen, the temperature variations across the computational domain remain relatively constant for all grid types. However, as the element size is decreased, we see a large temperature variation near the edge of the walls where two different boundary conditions meet. Additionally, for the multiblock girds, the transition between different blocks is evident. The transition from a fine grid to a coarse grid is not smoothed and therefore gives rise to computational errors.

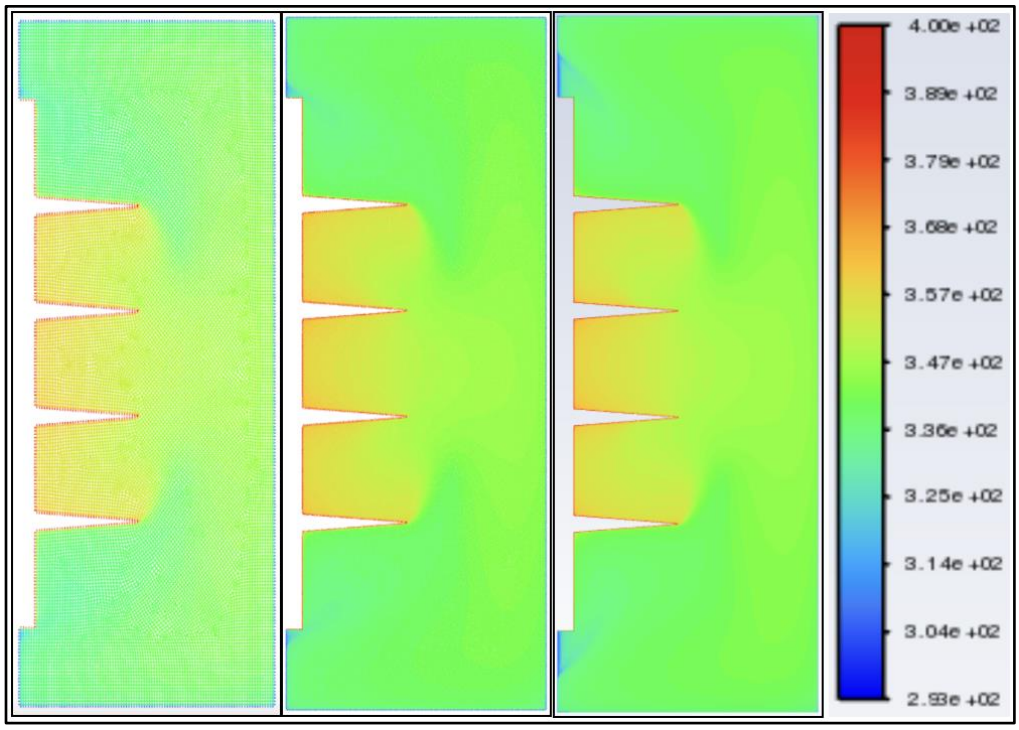

Figure 8: *Contours of Static Temperature in linear grids (Left: coarse, Center: medium, Right: fine).*

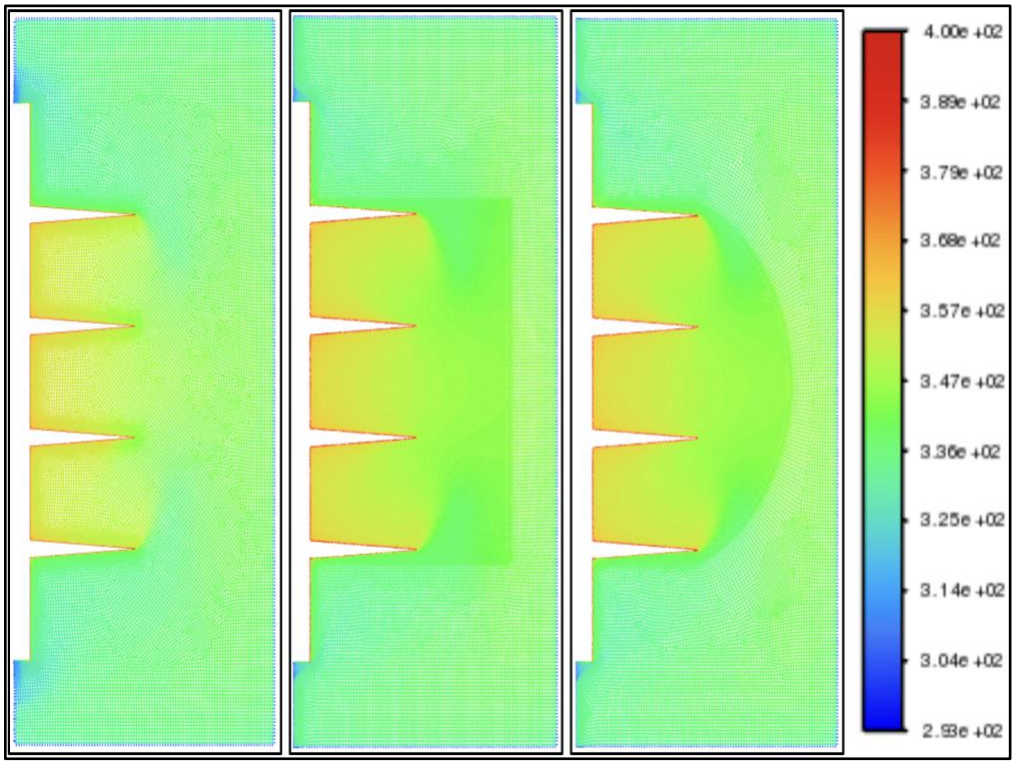

Figure 9: *Contours of Static Temperature in unstructured grids (Left: non-linear, Center: rectangular multiblock, Right: semicircular multiblock).*

Validation

For this computational analysis, a grid convergence study is performed for each characteristic parameter to ensure its asymptotic progress toward a grid-independent value. For this project, as discussed earlier, area-weighted average heat flux and the Nusselt number values are reviewed across the transient analysis for all grid types. A grid convergence study is performed to examine the variation of Nusselt number and heat flux across the three linear meshes developed in the previous section. **Table 9** tabulates the relative error, normalized error, and grid convergence index for the two characteristic parameters for this study.

Table 9: *Relative Error, Normalized Error, and Grid Convergence Index.*

No.	Relative Error	Normalized Error	GCI_{fine}
Nusselt No.			
f_2	0.0853	0.1906	0.2383
f_1	0.0626	0.1340	0.1749
Heat Flux			
f_2	0.0922	0.1400	0.1751
f_1	0.0589	0.0895	0.1118

As tabulated above, the relative error between a fine mesh and a medium mesh is approximately 6% for the Nusselt number, and the relative error for the same is 5% for the heat flux. The fine grid convergence index values of 0.175 and 0.112 are calculated for Nusselt number and heat flux respectively. Reflecting on the calculated relative and normalized, in my opinion, these values are larger than expected. To resolve this, meshes with even smaller element sizes should be evaluated.

Following this, Richardson's extrapolation is used to compute the grid-independent value for each characteristic parameter. A grid-independent heat flux was calculated to be -293.3 W/m^2, and a grid-independent Nusselt number was calculated to be 52.2.

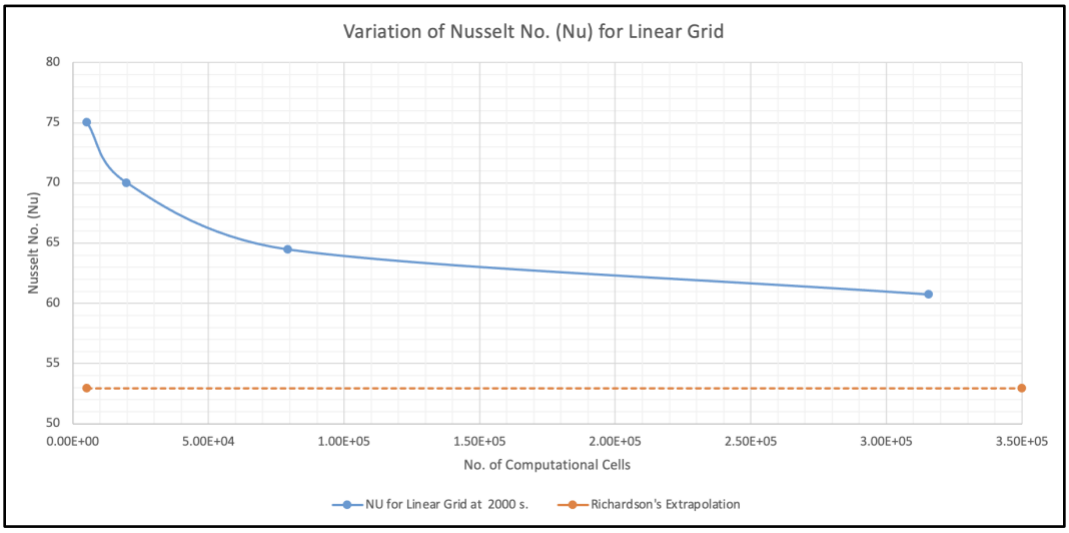

Figure 10: *Variation of Nusselt No for Linear Grid with Richardson's Extrapolation Solution.*

Figure 10 illustrates the variation of the Nusselt number for the three linear grids as a function of an increasing number of computational cells. **Figure 11** illustrates the variation of Heat flux for the three linear grids as a function of an increasing number of computational cells. For both characteristic parameters, as the number of computational cells increases, the respective parameter approaches its above-calculated grid-independent value.

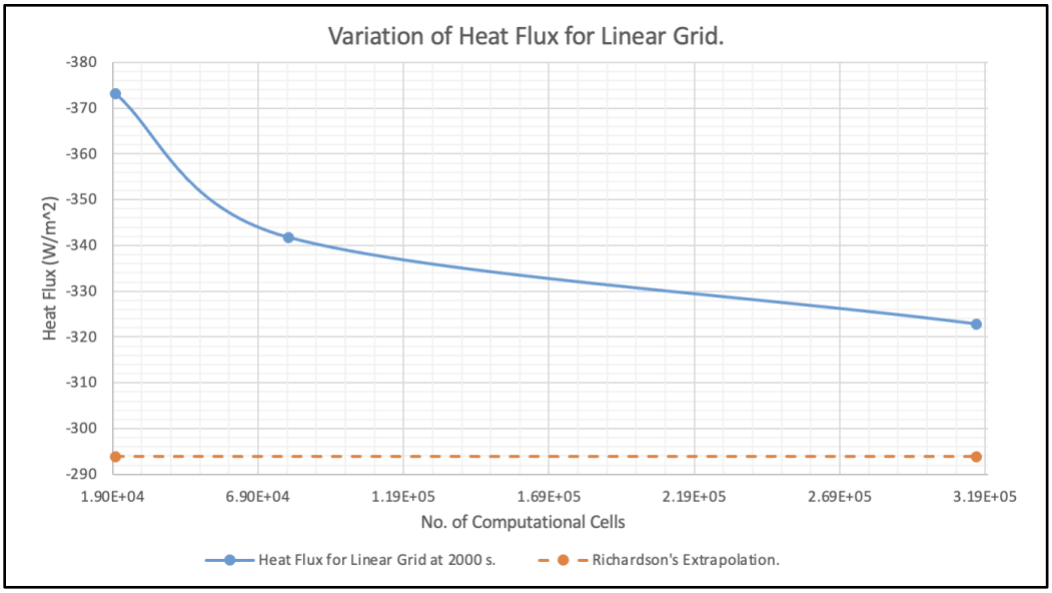

Figure 11: *Variation of Heat Flux for Linear Grid with Richardson's Extrapolation Solution.*

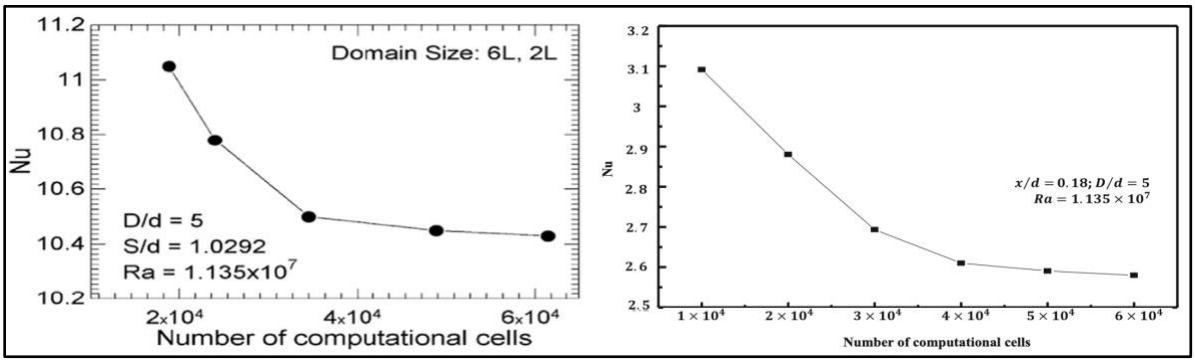

Figure 12: *Comparing to Historic Data (Left: Konijeti et al., Right: Senapati et al.) [5][1]*

Figure 12 illustrates the historical data for similar numerical simulations. The data sets are obtained from Konijeti et al. [5] (left) and Senapati et al. [1] (right). Konijeti et al. explore the heat transfer process over a vertical cylinder with triangular fins for various Rayleigh numbers and fin length-to-diameter ratios. Senapati et al. investigate the heat transfer process over a vertical cylinder with annular fins again for various Rayleigh numbers and fin length to diameter ratio. Comparing the Nusselt number variation with increasing computational cells in **Figure 10**, a clear trend is very evident. For the two historical plots in **Figure 12** and the results for this project in **Figure 10**, the Nusselt number is found to be decreasing with an increasing number of computational cells.

Discussion and Future Recommendations

While this study systematically explored the impact of various grid types and resolutions on the natural convection heat transfer process, several opportunities for further advancements remain unexplored due to time constraints. Future investigations could address the following areas to enhance the accuracy of the solution:

Implementing adaptive grid refinement techniques could significantly improve the efficiency and accuracy of simulations. In this approach, the computation would begin with a coarse mesh and adapt dynamically to the geometry based on flow features during the simulation. This would allow the mesh to concentrate cells in regions of high-temperature gradients or flow variations, reducing computational costs while maintaining solution accuracy.

Secondly, Exploring multiple time-stepping options is another area for improving simulation efficiency. Conducting a time-step convergence test could help evaluate the sensitivity of the heat transfer rate to time-step size and identify an optimal balance between temporal accuracy and computational effort. Such methods would also provide insights into transient phenomena that may not be resolved with uniform time steps.

Extending the analysis to include non-isothermal boundary conditions, such as linearly or non-linearly varying wall temperatures, could provide a more realistic representation of practical systems. This would require modifications to the numerical setup and could reveal additional complexities in the heat transfer behavior.

Conclusion

This study successfully investigated natural convection heat transfer over a vertical hollow cylinder with circular fins of triangular cross-section, employing various grid generation techniques and numerical approaches. The results highlighted the critical influence of grid resolution and mesh type on the accuracy of heat transfer simulations.

Structured grids with finer resolutions captured thermal gradients more accurately, with the finest linear mesh (element size = 0.05 m) achieving a Nusselt number of 60.75 and an average temperature of 343.6 K. However, this came at the expense of significantly increased computational time and computational cost, with the number of cells rising from 19,918 for the coarse grid to 315,720 for the fine grid.

Non-linear grids offered a balanced approach by concentrating cells near the heated cylinder walls, yielding a Nusselt number of 68.1, however, causing oscillations in the solution. These oscillations represented the influence of turbulent and laminar flow inside the boundary layer as time increases. Meanwhile, multi-block grids demonstrated their utility in optimizing computational performance without substantial loss in accuracy, with both rectangular and semi-circular configurations producing consistent Nusselt numbers of approximately 68.8.

The study also validated its results through a grid convergence index (GCI) analysis, ensuring grid independence with GCI values of 0.175 and 0.112 for the Nusselt number and heat flux, respectively. A grid-independent heat flux was calculated to be -293.3 W/m^2, and a grid-independent Nusselt number was calculated to be 52.2. Comparison to historical data from Senapati et al. and Konijeti et al. revealed agreement in trends, with the Nusselt number decreasing as mesh refinement increased.

In conclusion, this investigation focuses on the importance of grid design and refinement in resolving transient natural convection phenomena while managing computational demands. These findings provide a foundation for more advanced techniques, such as adaptive mesh refinement and multi-time-stepping approaches, to further optimize the balance between accuracy and efficiency in numerical heat transfer simulations.

Appendix

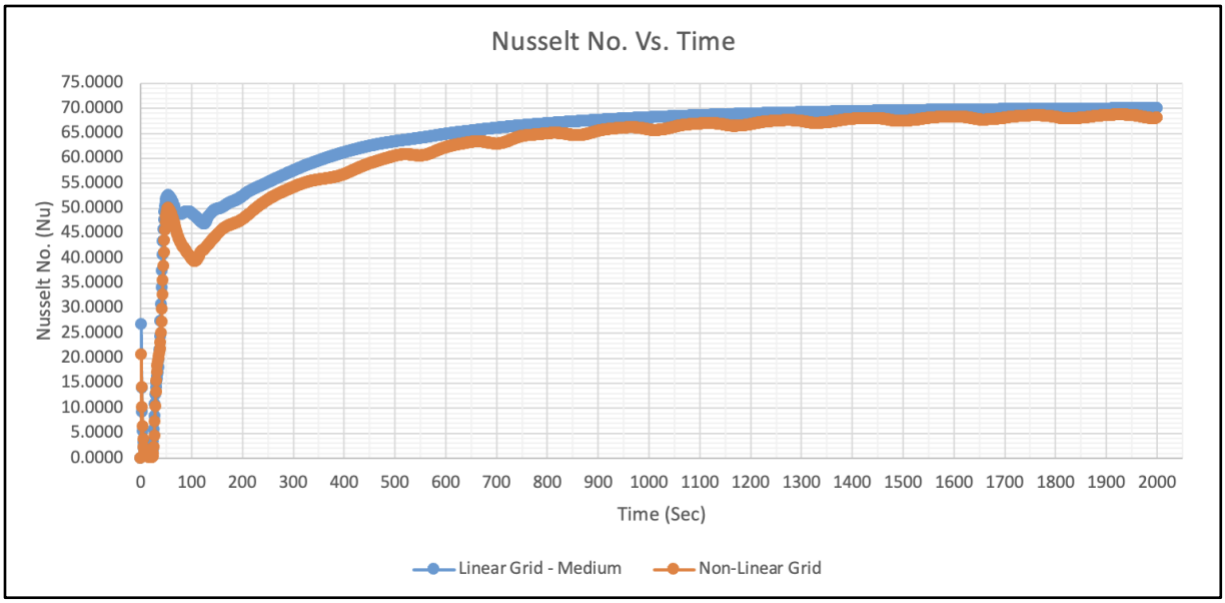

Figure 13: *Nusselt number vs. time for a linear coarse mesh and non-linear grid.*

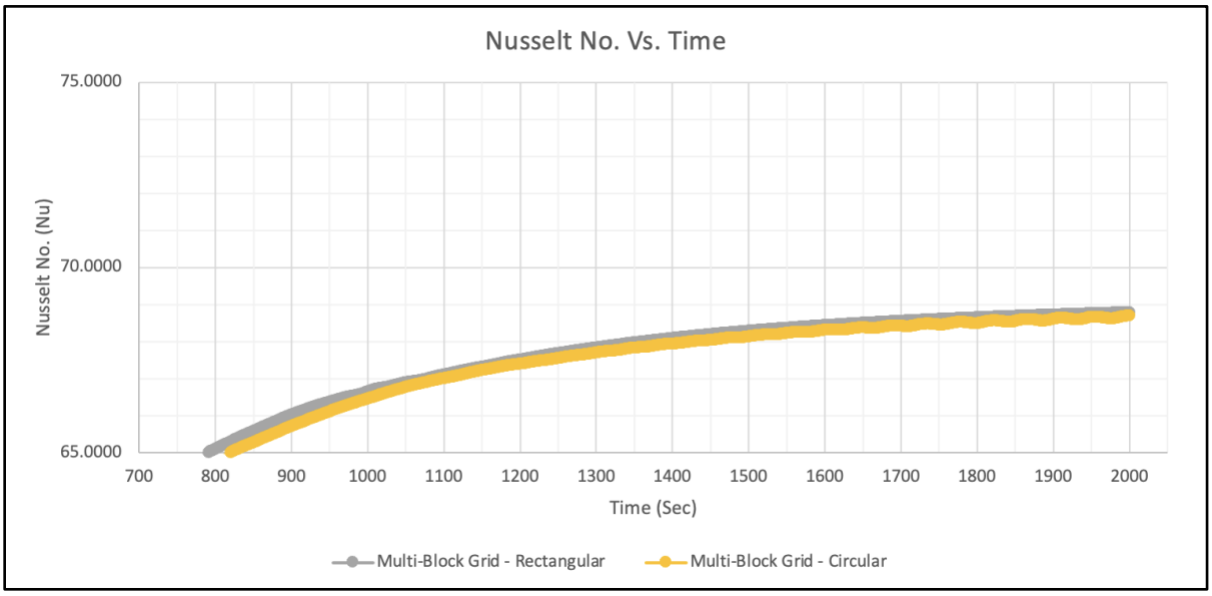

Figure 14: *Zoomed-in figure of Nusselt number vs time for the multiblock grids.*

Structured Grid					Unstructured Grid				
mesh	cells	temp	heat flux	NU	mesh	cells	temp	heat flux	NU
coarse	19918	343.8	-373.3	70	non-linear	45704	340.6	-340.5	68.1
medium	79289	343.5	-341.8	64.5	multiblock - rectangular	51153	342	-353.6	68.8
fine	315720	343.6	-322.8	60.7	multiblock - semicircular	47277	341.9	-353	68.7
Richardson Extrapolation			-293.92	52.20588235					

Grid Convergence Index				
r	2		relative error	
ln_(r)	0.69314718	coarse	0.09215916	0.085271318
p_NU	0.5334322	fine	0.05885998	0.062602965
p_heatflux	0.72935241		Absolute error	
Fs	1.25	coarse	0.14008192	0.190606475
		fine	0.08946716	0.13993604
			GCI Fine	
		coarse	0.1751024	0.238258094
		fine	0.11183395	0.17492005

Figure 15: *Grid Convergence sample calculations.*

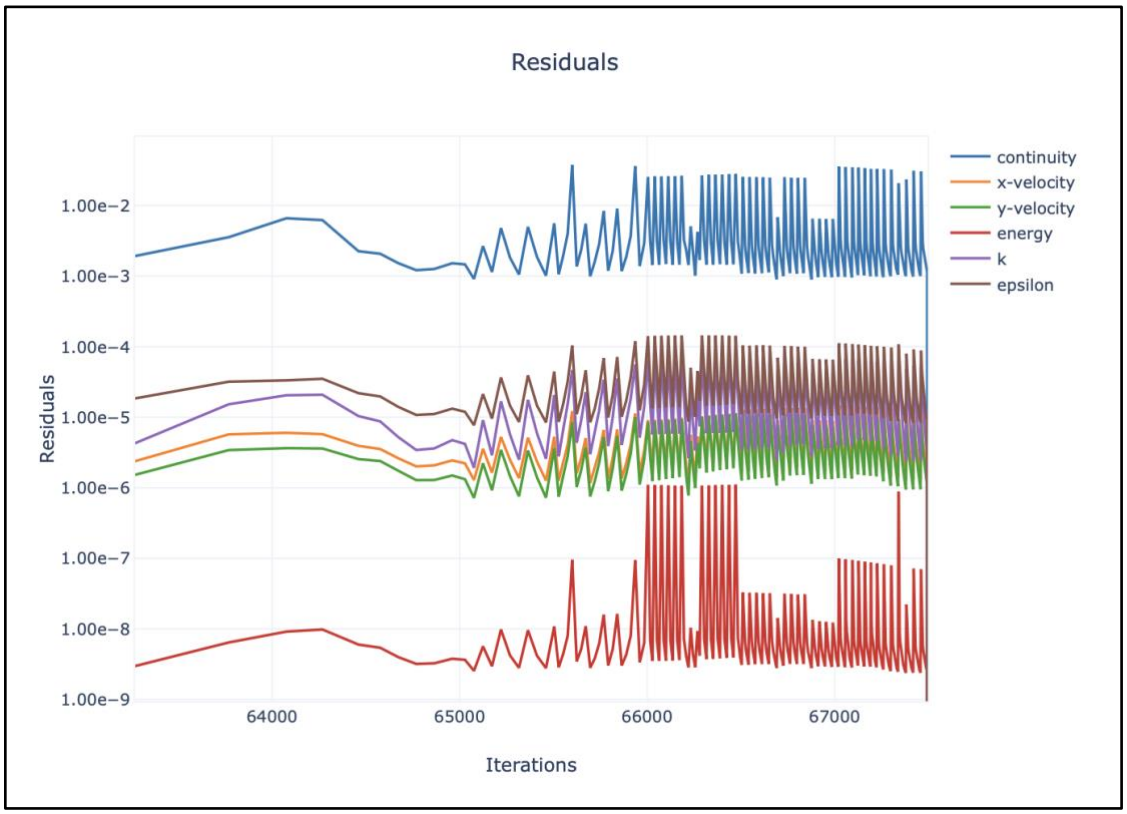

Figure 16: *Residuals - Nonlinear grid.*

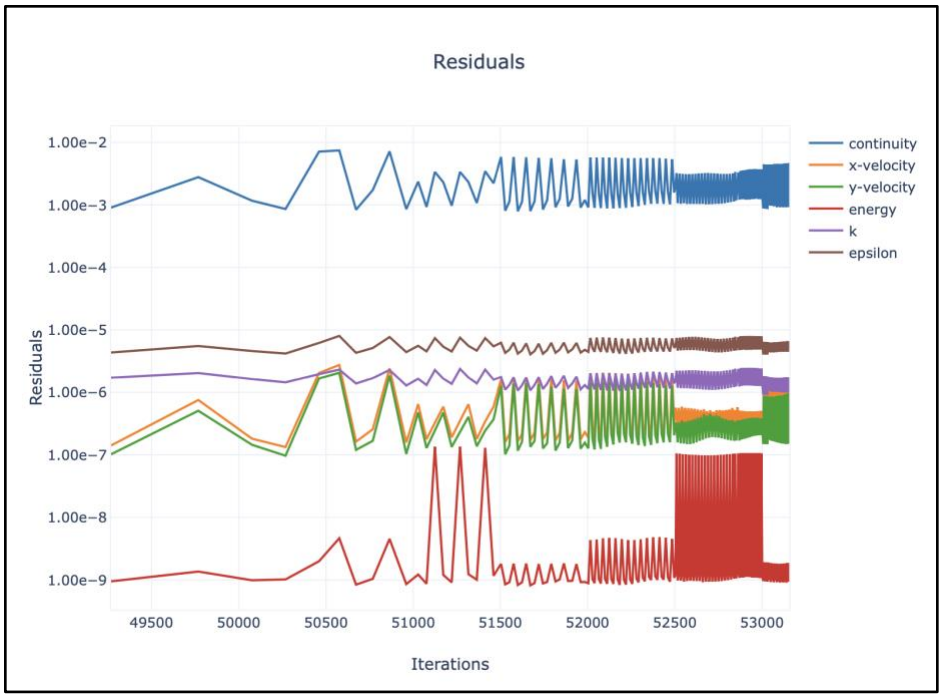

Figure 17: *Residuals – Rectangular Multiblock grid.*

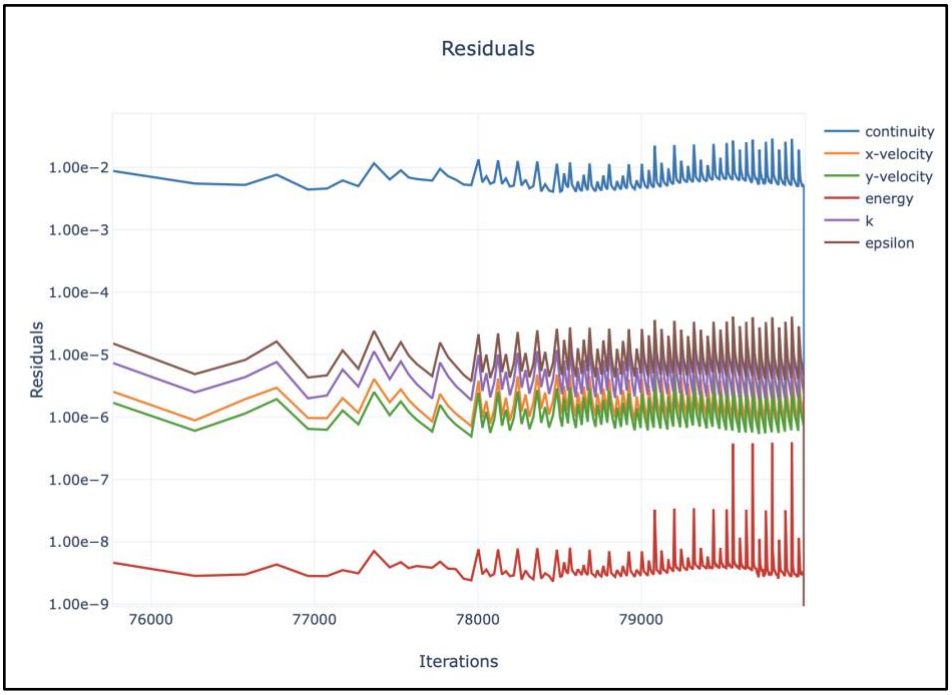

Figure 18: *Residuals – Semi-circular Multiblock grid.*

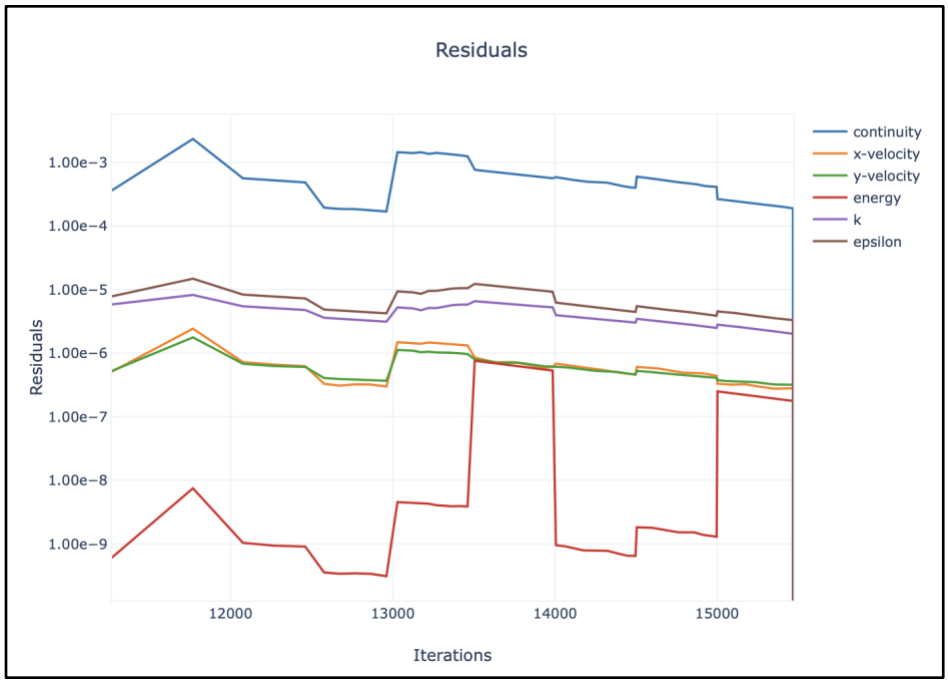

Figure 19: *Residuals – Coarse Linear Mesh.*

Figure 20: *Residuals – Medium Linear Mesh.*

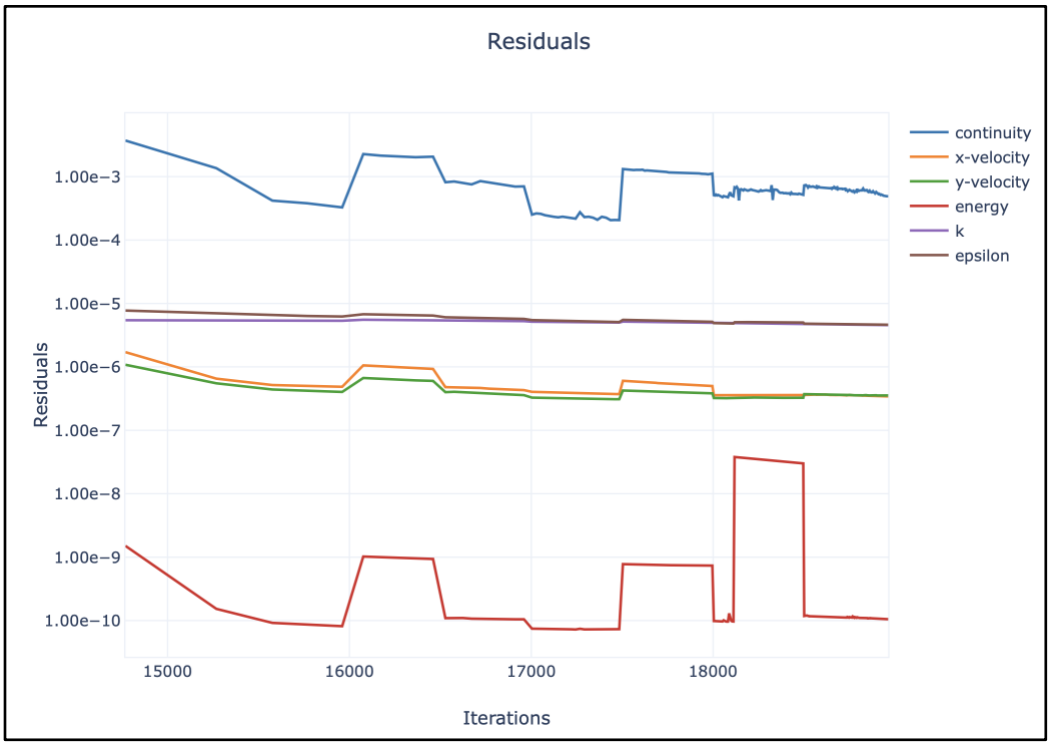

Figure 21: *Residuals – Fine Linear Mesh.*

References

[1] J. R. Senapati, S. K. Dash, and S. Roy, "Numerical investigation of natural convection heat transfer from a vertical cylinder with annular fins," International Journal of Thermal Sciences, vol. 111, pp. 146–159, 2017, doi: 10.1016/j.ijthermalsci.2016.08.019

[2] B. H. An, H. J. Kim, and D.-K. Kim, "Nusselt number correlation for natural convection from vertical cylinders with vertically oriented plate fins," Experimental thermal and fluid science, vol. 41, pp. 59–66, 2012, doi: 10.1016/j.expthermflusci.2012.03.010

[3] K. Kitamura and F. Kimura, "Heat transfer and fluid flow of natural convection adjacent to upward-facing horizontal plates," International journal of heat and mass transfer, vol. 38, no. 17, pp. 3149–3159, 1995, doi: 10.1016/0017-9310(95)00066-I

[4] S. Acharya, S. Agrawal, and S. K. Dash, "Numerical Analysis of Natural Convection Heat Transfer From a Vertical Hollow Cylinder Suspended in Air," Journal of heat transfer, vol. 140, no. 5, 2018, doi: 10.1115/1.4038478

[5] R. Konijeti, A. Dasore, U. Rajak, R. Kumar, A. Sharma, and A. S. Yadav, "CFD analysis of heat transfer by free convection over a vertical cylinder with circular fins of triangular cross-section," Multiscale and Multidisciplinary Modeling, Experiments and Design, vol. 7, no. 2, pp. 741–753, 2024, doi: 10.1007/s41939-023-00237-x

[6] H.-T. Chen and J.-C. Chou, "Investigation of natural-convection heat transfer coefficient on a vertical square fin of finned-tube heat exchangers," International Journal of heat and mass transfer, vol. 49, no. 17, pp. 3034–3044, 2006, doi: 10.1016/j.ijheatmasstransfer.2006.02.009

[7] M. K. Dash and S. K. Dash, "Natural convection heat transfer and fluid flow around a thick hollow vertical cylinder suspended in the air: A numerical approach," International journal of thermal sciences, vol. 152, pp. 106312-, 2020, doi: 10.1016/j.ijthermalsci.2020.106312

[8] B. Singh and S. K. Dash, "Natural convection heat transfer from a finned sphere," International Journal of heat and mass transfer, vol. 81, pp. 305–324, 2015, doi: 10.1016/j.ijheatmasstransfer.2014.10.028

[9] I. Tari and M. Mehrtash, "Natural convection heat transfer from inclined plate-fin heat sinks," International Journal of heat and mass transfer, vol. 56, no. 1–2, pp. 574–593, 2013, doi: 10.1016/j.ijheatmasstransfer.2012.08.050